A MOVING MAGNET ACTUATOR FOR LARGE RANGE NANOPOSITIONING

G. Parmar*, D.B. Hiemstra, Y. Chen and S. Awtar
Precision Systems Design Laboratory
Mechanical Engineering, University of Michigan
Ann Arbor, Michigan 48109

ABSTRACT

In this paper, we present the design, fabrication, and testing of a moving magnet actuator (MMA) for large range (∼10mm) nanopositioning. MMAs are direct-drive, single-phase electromagnetic linear actuators that provide frictionless and backlash-free motion. These qualities, along with an adequate motion range, make MMAs promising candidates for large range nanopositioning. In this work, we identify actuator- and system-level performance criteria and associated design tradeoffs, and use this knowledge to systematically and concurrently design an MMA and a double parallelogram flexure bearing. The resulting actuator provides a force output per unit square root power of $4.56N/\sqrt{W}$, better than 9% force uniformity with respect to stroke, and a low moving mass of 106g. An integrated thermal management system is also incorporated as part of the actuator in order to mitigate the heat dissipated from the MMA coils. The overall single-axis motion system was fabricated and tested to demonstrate a 36Hz open-loop bandwidth and less than 4nm (RMS) steady-state positioning noise over a 10mm motion range. Preliminary closed-loop design and testing highlight the potential of the proposed actuator in nanopositioning.

INTRODUCTION AND MOTIVATION

A moving magnet actuator (MMA) is a direct-drive, single phase, electromagnetic linear actuator. MMAs have been employed in the past in a wide range of applications including disk drives, automotive valves, and vibration isolators [1–3]. A commonly used MMA architecture is shown in Fig. 1, where an axially-oriented cylindrical permanent magnet sandwiched between two iron pole-pieces forms the mover. The stator consists of a back iron along with two oppositely wound coils connected in series. The magnetic field due to the magnet produces a Lorentz force on the mover, proportional to the coil current. The fact that MMAs provide non-contact frictionless actuation over several millimeters makes them a potential candidate for actuation in large range nanopositioning systems.

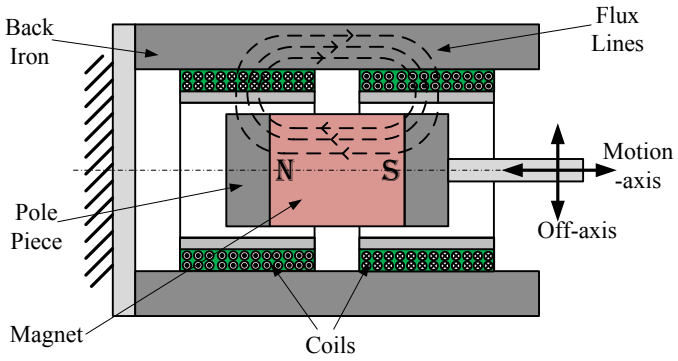

Figure 1. A MOVING MAGNET ACTUATOR SCHEMATIC.

A nanopositioning system is a mechatronic motion system capable of providing nanometer-level precision (repeatability of motion), accuracy (lack of error in motion), and resolution (minimum incremental motion). Nanopositioning systems with large range capability (∼10mm) are becoming increasingly desirable in a variety of applications including scanning probe microscopy, nanometrology, nanolithography, hard-drive and semiconductor inspection, and memory storage [4–6]. However, most existing nanopositioning systems are generally limited to a few hundred microns of motion range [6]. The fundamental challenge in simultaneously achieving large motion range and nanometric motion quality (precision, accuracy, and resolution) in a nanopositioning system lies mainly in the limitations of existing individual components (i.e., bearing, actuator, sensor) and their integra-

*Corresponding Author (parmar@umich.edu, 734-239-2928)

tion [7]. While flexure, magnetic, and air bearings provide good choices for motion-guidance, the actuator itself has to be capable of large range and nanometric motion quality. Piezoelectric stack actuators have been the most common choice for nanopositioning due to their frictionless motion and large bandwidth, but they have an inherently small stroke ($<$200μm) [6,8]. Inchworm-type actuators, which are capable of providing large motion range with small motion steps ($\sim$10nm), do not provide a continuous smooth motion and lack sufficient operating speeds [8]. Non-contact direct-drive multi-phase electromagnetic linear motors are capable of providing large motion range, but suffer from magnetic hysteresis and cogging, which limits their precision [9]. A simpler electromagnetic actuator, namely, the voice coil, has also been used because of its non-contact, cog-free motion characteristics [10, 11]. Although a voice coil actuator (VCA) provides a smaller motion range ($\sim$10mm) compared to a linear motor, it is sufficient for the above-listed large range nanopositioning applications. However, heat dissipation from the coil connected to the motion stage and non-deterministic disturbance due to the moving cables degrade the accuracy and precision of the nanopositioning system. To overcome these problems, some researchers have used the voice coil in an inverted configuration, i.e., by using the coil as the stator and the magnet and back-iron as the mover [12, 13]. However, this approach adds a relatively large mass to the motion stage, which in turn limits the motion system's dynamic performance (i.e., open-loop and closed-loop bandwidth).

While, in principle, the operation of an MMA is similar to a VCA used in an inverted configuration, the key difference in this case is that the relatively heavy back-iron is attached to the static coils and not to the magnet. Thus, the moving mass is greatly reduced while still maintaining the benefits of the inverted VCA configuration. The non-deterministic disturbance due to the moving cables is eliminated, making it a truly non-contact actuator. Furthermore, the coils are connected to the static ground frame as opposed to the mover, which allows for better heat dissipation and keeps the heat generated due to resistive losses in the coils further away from the motion stage. However, unlike VCAs, MMAs exhibit greater non-uniformity in force over the stroke. Also, separating the back iron from the permanent magnet introduces a potential instability in the direction perpendicular to the motion axis [14]. To address these actuator-specific as well as other system-level design challenges, we develop an analytical model for the traditional MMA architecture of Fig. 1 integrated with a flexure bearing. We then identify fundamental performance trade-offs in terms of the material and geometry choices for the actuator and flexure bearing. Based on this understanding, we designed and fabricated an optimal motion system for large range nanopositioning. An integrated thermal management system is also incorporated to effectively dissipate the heat generated by the MMA coils. A preliminary closed-loop controller is implemented to demonstrate less than 4nm (RMS) steady-state positioning noise over a 10mm motion range.

SYSTEM LEVEL PERFORMANCE CRITERIA AND TRADE-OFFS

The MMA and the flexure bearing are designed concurrently in order to meet the following system-level quasi-static performance criteria:

I. Maximize the first natural frequency (or open-loop bandwidth), which is directly related to the practically achievable speed and disturbance rejection of the motion system in closed-loop operation. This criterion requires increasing the motion-direction bearing stiffness and the continuous force output of the actuator, and decreasing the overall moving mass.

II. Minimize the power consumption of the actuator. During quasi-static operation, all the power consumed is dissipated as heat. This heat is detrimental to the performance of the feedback sensor, which can degrade the accuracy of the overall motion system. Furthermore, for a given a maximum power consumption, the maximum current should be reduced by increasing the maximum voltage. This is beneficial because drive-amplifiers exhibit less distortion for lower current levels.

III. Maximize the uniformity of force with respect to the position of the mover. Potential non-uniformities are generally non-linear in nature and can compromise the open-loop as well as closed-loop tracking performance of the motion system.

IV. Ensure that the off-axis attraction between the magnet and the back iron does not cause the moving magnet to pull in sideways to the stator. To avoid this sideways instability, the flexure bearing has to provide a higher positive off-axis stiffness compared to the negative (or destabilizing) off-axis stiffness associated with the magnetic force between the moving magnet and the back iron.

As explained in the following discussion, it is not possible to simultaneously satisfy all of the above-mentioned performance criteria. In particular, the force output of an MMA can be increased by either increasing the moving mass or by increasing the quasi-static power consumption limit, both of which are undesirable. Although such a trade-off in MMAs has been identified in previous work, the discussion has been mostly qualitative [15, 16]. To quantitatively determine the effect of geometric scaling on the actuator output force, power consumption, and moving mass, we consider a lumped parameter model of the traditional MMA architecture in Fig. 2. The following assumptions are made to simplify the analysis: a) Any fringing and leakage flux is neglected. b) The reluctance of the back iron and pole pieces is neglected. c) The relative permeability of the magnet is assumed to be equal to that of air; and d) All the space between the pole pieces and the back iron is occupied by coils. Dimensions l_m, l_p, r_m, and t_g denote the nominal magnet length, pole piece length, magnet radius, and air gap thickness, respectively. The variable α is a multiplicative scaling factor applied to these nominal dimensions to study the effect of the actuator's size on its performance.

Referring to Fig. 2, the magneto-motive force (F_m) and the lumped reluctances of the magnet and the air gap (R_m and R_g) are given by

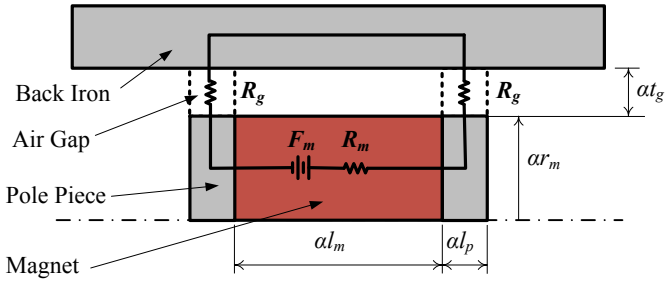

Figure 2. SIMPLIFIED LUMPED PARAMETER MMA MODEL.

$$F_m = \frac{\alpha B_r l_m}{\mu_m}; \quad R_m = \frac{l_m}{\pi\alpha\mu_m {r_m}^2}; \quad R_g = \frac{1}{2\pi\alpha\mu_0 l_p}\ln(1+\frac{t_g}{r_m}) \quad (1)$$

where B_r and μ_m denote the remanent flux density and the permeability of the permanent magnet, respectively, and μ_0 represents the permeability of air. The resultant flux (ϕ) and average magnetic flux density in the air gap (B_g) is then given by

$$\phi = \frac{F_m}{R_m + 2R_g}; \quad B_g = \frac{\phi}{2\pi\alpha^2 l_p (r_m + t_g/2)} \quad (2)$$

For a given coil current (i), the force output (F), the power consumed (P), and the moving mass (m_a) can be determined to be

$$\begin{aligned} F = B_g i l_w = B_g i \frac{4\pi\alpha^3 l_p t_g (r_m + t_g/2)}{d^2} \\ P = i^2 R = \frac{\rho_c l_w}{A_w} = i^2 \rho_c \frac{16\alpha^3 l_p t_g (r_m + t_g/2)}{d^4} \\ m_a = \rho_m \pi \alpha^3 {r_m}^2 l_m \end{aligned} \quad (3)$$

where R is the coil resistance, ρ_c is the resistivity of the coil wire, d is the wire diameter, A_w is the cross-sectional area of the wire, l_w is the total length of the wire in the air gap, and ρ_m is the mass density of the magnet. These three relations lead to

$$\frac{F}{\sqrt{P}\sqrt{m_a}} = \frac{B_r}{\frac{l_m l_p}{{r_m}^2} + ln(1+\frac{t_g}{r_m})} \sqrt{\frac{\pi l_m l_p t_g}{4\rho_c \rho_m {r_m}^2 (r_m + t_g/2)}} \quad (4)$$

In the above relation, the scaling factor α, wire diameter d, and coil current i get canceled out, and the right hand side term is only dependent on the physical constants and nominal dimensions, which are constant for a given MMA architecture. Thus, the force output (F) remains directly proportional to the square root of the actuator moving mass (m_a) and the square root of power consumed (P), irrespective of the scale of the actuator (α). Equation (4) may be restated as follows

$$\frac{F}{\sqrt{P}\sqrt{m_a}} = \frac{K_t}{\sqrt{R}\sqrt{m_a}} \triangleq \beta \text{ (constant)} \quad (5)$$

where K_t is the force constant (force per unit current) of the MMA. Although several simplifying assumptions were made in the derivation of this relation, it is found to be true even when these assumptions are relaxed in a finite element analysis (FEA) conducted in Maxwell^{TM}, as shown in Fig. 3. The ratio $K_t/\sqrt{R}$, also referred to as the actuator constant, is plotted against $\sqrt{m_a}$ for different values of the scaling factor α. It is evident that, for the given MMA architecture, the ratio between the actuator constant and square root of the actuator moving mass turns out be a constant (β), irrespective of the size of the actuator (i.e., value of α).Therefore, the constant β (units of $\sqrt{\text{Hz}}$), proves to be an important figure of merit in the design of an MMA.

An important consequence of Eq. (5), when an MMA is used with a flexure bearing, is that it limits the first natural frequency and therefore the open-loop bandwidth (ω_n) of the overall motion system. Consider a flexure bearing with motion-direction stiffness (K_y) and motion stage mass (m). The maximum continuous force generated by the MMA must satisfy

$$K_t i_{max} = K_y \Delta \quad (6)$$

where i_{max} is the current corresponding to a given maximum power consumption limit (P_{max}), and Δ represents the desired unidirectional motion range. Then, ω_n is given by

$$\begin{aligned} {\omega_n}^2 &\approx \frac{K_y}{(m+m_a)} = \frac{K_t i_{max}}{\Delta(m+m_a)} = \frac{K_t\sqrt{P_{max}}}{\Delta\sqrt{R}(m+m_a)} \\ &< \beta \frac{\sqrt{P_{max}}}{\Delta} \frac{\sqrt{m_a}}{(m+m_a)} \end{aligned} \quad (7)$$

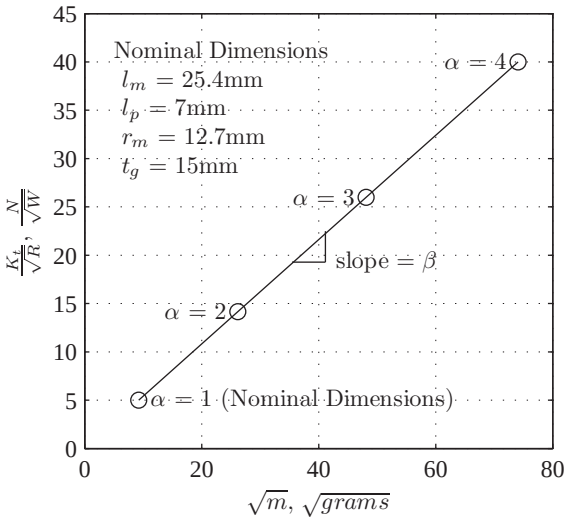

Figure 3. EFFECT OF GEOMETRIC SCALING ON THE PERFORMANCE OF AN MMA.

Hence, for a given architecture of the MMA (i.e., given β) and with a power consumption limit (P_{max}) and specified motion range (Δ), the open-loop bandwidth of the motion system has an upper bound, which depends on the moving mass of the actuator. For example, if the flexure bearing is designed to be stiffer in hope of increased bandwidth, it would also require an increase in the actuation force in order to retain the same motion range. However, as per Eq. (5), this can only be achieved by increasing the moving magnet mass, for a fixed power consumption limit. Therefore, using a stiffer bearing will not lead to an increase in the open-loop bandwidth. The above relation is also critical from a feedback control system design standpoint since a limit on the natural frequency of the motion system also limits the achievable bandwidth and disturbance rejection in closed-loop operation [17].

It is therefore evident that in order to maximize the open-loop bandwidth of the motion system based on an MMA and flexure bearing, one has to maximize the constant β while keeping the moving mass as small as possible. In this work, the motion range was set to be ±5mm, and power and voltage limit of 20W and 25V, respectively, were based on a custom-made low-noise drive amplifier developed in our laboratory.

MMA DESIGN AND FABRICATION

The design of the actuator was carried out in a step-wise manner in order to maximize the constant β while maintaining acceptable force uniformity (better than 10%) over the ±5mm stroke of the actuator. It can be separately shown that although removing the pole pieces reduces the force constant (K_t), it leads to an overall higher value of β due to the reduced moving mass. As a result, the pole pieces were eliminated in our design, which is schematically illustrated in Fig. 4, along with the key geometrical dimensions. All the results presented in the following design steps are based on quasi-static FEA in Maxwell™.

1. The minimum magnet length (l_m) is governed by the stroke (Δ) and the coil separation (l_g), i.e.,

$$l_m \geq 2\Delta + l_g \tag{8}$$

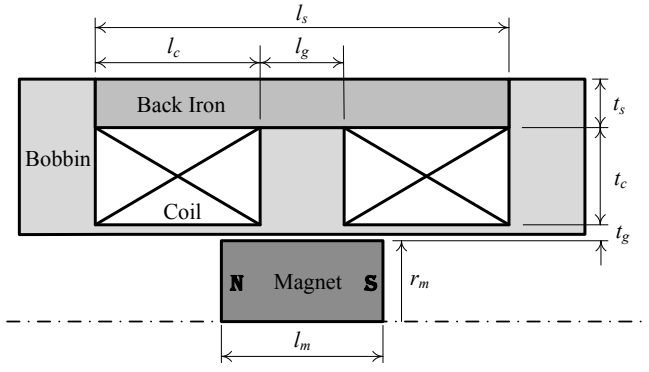

Figure 4. MMA ARCHITECTURE WITH KEY DIMENSIONS.

The coil separation (l_g) was selected so that the fringing flux from one face of the magnet does not pass through the opposite coil (for a reasonable coil radial thickness), when the magnet is at the end of the stroke. This would otherwise lead to reduced uniformity of the force over the stroke. With the 5mm stroke (Δ) and a minimum coil separation (l_g) of 10mm, the magnet length (l_m) was, therefore, chosen to be 25.4mm. This also places a limitation on the minimum moving mass of the actuator. It must be noted that the magnet dimension is also influenced by the standard sizes that are commercially available.

2. Once the magnet length is chosen, the magnet radius (r_m) and the coil thickness (t_c) can be optimized to obtain the required actuator constant ($K_t/\sqrt{R}$), while keeping the magnet mass as low as possible (to maximize β). The actuator constant needed in this case is approximately $4\text{N}/\sqrt{\text{W}}$ for a force requirement of 17N (based on the bearing design presented later) and power constraint of 20W. Figure 5A shows the effect of varying the magnet radius and coil thickness on the actuator constant. Based on this plot, r_m and t_c were chosen to be 12.7mm and 15mm, respectively, to achieve an actuator constant of $4.5\text{N}/\sqrt{\text{W}}$. This resulted in a β value of $14\sqrt{\text{Hz}}$.

3. Assuming the width of the flux path is approximately equal to the radius of the magnet, the coil length (l_c) is dictated by the stroke and the magnet radius as follows

$$l_c \geq 2\Delta + r_m \tag{9}$$

Increasing the length of the coil improves the uniformity but only at the cost of an increase in the coil resistance, which reduces the actuator constant (and β). As shown in Fig. 5B, the coil length was chosen to be 26mm to limit the drop in force constant at the ends of the stroke to be less than 10% without any appreciable loss in the actuator constant.

4. As shown previously in Eq. (4), the actuator constant is only dependent on the volume of the coil and is independent of the wire diameter (d). However, the diameter of the wire can be chosen to minimize the maximum continuous current requirement as long as the voltage constraint is met. This is beneficial since current drivers usually show higher noise and distortion for higher current levels. This tradeoff is shown in Fig. 5C, based on which 25AWG wire, with a diameter of 0.455mm, was chosen. This resulted in a coil resistance of 43.6Ω and a maximum continuous current requirement of 0.56A.

5. The thickness of the back iron (t_s) is governed by the requirement that the magnetic flux density in the iron should be below saturation for all values of coil current. Also, a larger length of the back iron (l_s) decreases the axial magnetic force between the magnet and the back iron. Since this force is undesirable, it is beneficial to increase the length of the back iron.

Table 1 summarizes the final dimensions of the MMA. The magnetic flux density and the flux lines at the zero stroke position are shown in Fig. 6. The magnetic flux density in the coil lies between 0.1T and 0.3T. Although the flux density is relatively

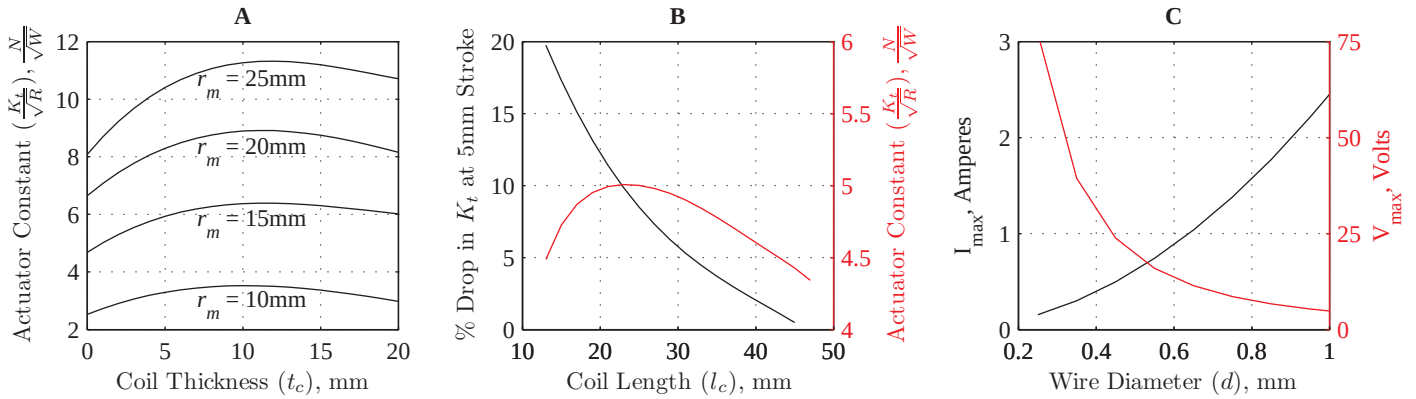

Figure 5. MMA DESIGN TRADES-OFFS: (**A**). ACTUATOR CONSTANT OF THE MMA FOR VARYING COIL THICKNESS AND MAGNET RADIUS. (**B**). PERCENTAGE DROP IN FORCE CONSTANT AT THE ENDS OF THE STROKE AND ACTUATOR CONSTANT VS. COIL LENGTH. (**C**). MAXIMUM CONTINUOUS CURRENT AND VOLTAGE REQUIREMENT VS. WIRE DIAMETER.

low, the large coil volume ensures a good force output of the MMA.

The resulting force generated by the MMA for zero and non-zero coil current is shown in Fig. 7. This force on the mover (i.e., the magnet) is the summation of two components. One is the Lorentz force between the current-carrying coil and the magnet. The drop in this force component towards the ends of the stroke can be attributed to the finite axial length of the coils and is less than 9% over a stroke of 10mm. The other component is the axial force on the magnet from the ferromagnetic back iron which acts as a magnetic spring and tends to restore the magnet to the center of the stroke. This force can be explicitly plotted for the case when there is no current flowing through the coils. It is important to note that the force between the magnet and the back iron is specific to MMAs and is not seen in the case of VCAs, in which the back iron and the magnet are rigidly attached together. The magnitude of this component can be minimized by increasing the axial length of the back iron. While the Lorentz force component is symmetric with respect to zero stroke position, the overall force profile turns out to be non-symmetric due to the force between the magnet and the back iron.

Table 1. KEY MMA DIMENSIONS.

Parameter	**Symbol**	**Value***
Magnet Axial Length	l_m	25.4
Magnet Radius	r_m	12.7
Coil Axial Length	l_c	26.0
Coil Radial Thickness	t_c	15.0
Back Iron Radial Thickness	t_s	7.6
Back Iron Axial Length	l_s	65.0
Gap Between Coil Stacks	l_g	13.2
Mechanical Air Gap	t_g	0.5
Wire Diameter	d	25 AWG

* All Dimensions are in mm.

Based on the MMA design presented above, various components were fabricated and assembled as shown in an exploded view in Fig. 8. A Neodymium-Iron-Boron (NdFeB grade N52) axial magnet is used because of its high remanent magnetization of 1.45T, which provides a high actuator constant for the MMA ($K_t/\sqrt{R} \propto B_r$). This magnet grade has a low Curie Temperature (80°C), but with the thermal management system described in the next section, this risk was mitigated. The magnet is mounted on a tubular carbon fiber shaft using nylon sleeve collars. Carbon fiber is lightweight and has good stiffness and strength properties. For the coil, 25AWG copper wire is wound on an Aluminum bobbin. Aluminum is chosen because of its good machinability and high thermal conductivity. Also, it acts as a shorted turn which reduces the coil inductance [18]. The back iron is manufactured from 1020C steel with a saturation flux density of 1.6T.

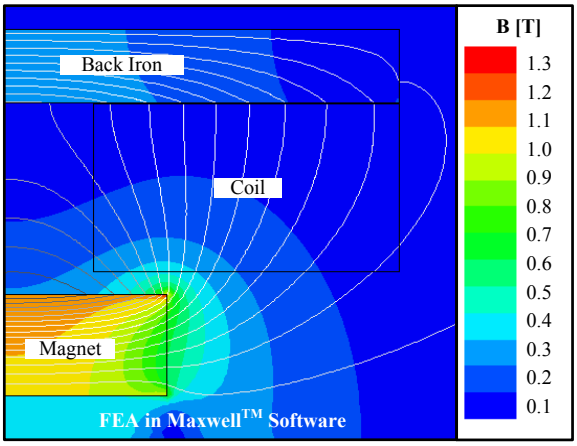

Figure 6. MAGNETIC FLUX DENSITY AND FLUX LINES IN THE MMA.

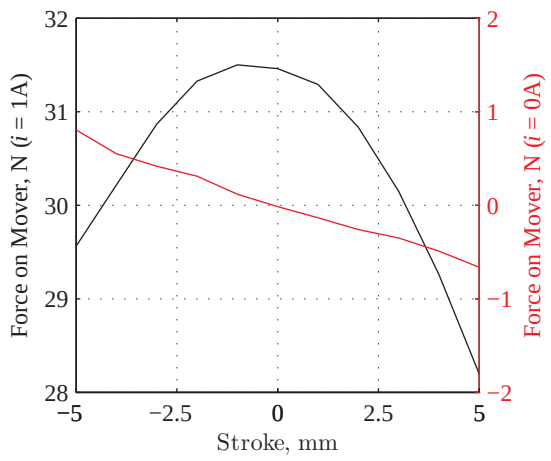

Figure 7. MOVER FORCE VS. STROKE FOR I = 0A AND I = 1A COIL CURRENT.

To simplify the assembly process, the back iron is designed as two symmetric halves so that the magnet and the bobbin can be easily assembled *a priori* without the iron being in the vicinity of the strong magnetic force generated by the permanent magnet.

THERMAL MANAGEMENT SYSTEM

In order to ensure that the heat generated by the MMA coils does not affect the remanence of the permanent magnet, the motion stage of the flexure bearing, or the accuracy of the position sensor, a passive thermal management system (TMS) was incorporated in the actuator design. It provides an effective way to transfer heat from the MMA coils to an ice pack via heat pipes. This method is advantageous as compared to other convective heat dissipation methods, which may lead to air flow-induced vibrations.

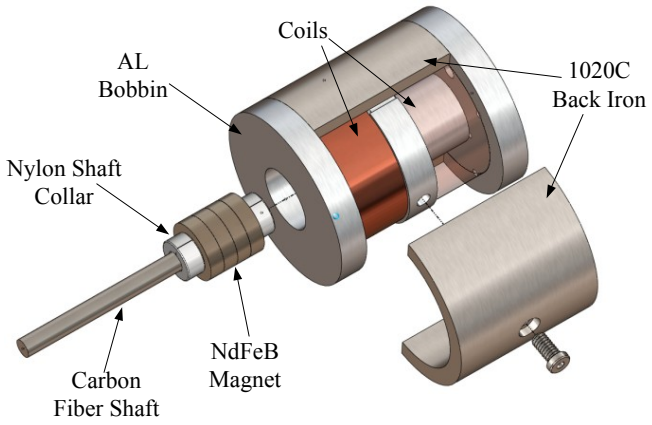

Figure 8. EXPLODED VIEW OF THE MMA.

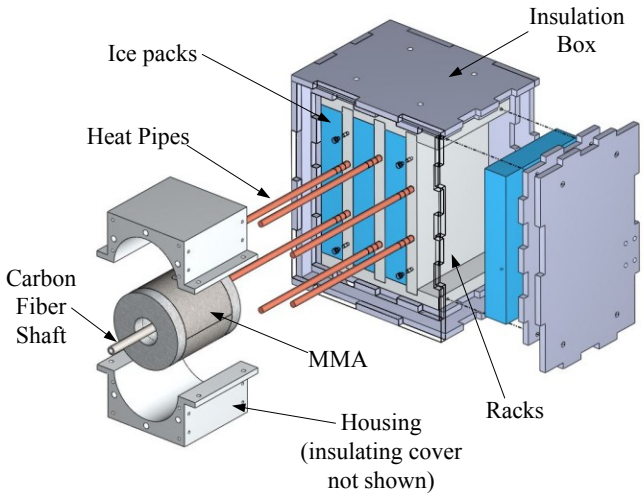

Figure 9. THERMAL MANAGEMENT SYSTEM.

An exploded view of the TMS is shown in Fig. 9. The Aluminum bobbin was designed to effectively transfer the heat radially outwards from the coils. The Aluminum housing around the back iron and coil bobbin is made in two symmetrical halves and provides a conductive interface between the actuator and copper heat pipes. The other ends of the heat pipes are inserted into a heat exchange unit, which consists of Aluminum racks stacked with ice packs. The Aluminum housing and the heat exchange unit are thermally insulated via a double-layered acrylic box in order to minimize any thermal fluctuations of the surrounding environment. The carbon fiber shaft used to interface the MMA with the motion stage of the flexure bearing provides low thermal conductivity and therefore acts as an effective heat barrier.

The critical components of the TMS (heat pipes, ice packs, and Aluminum racks) were designed in order to ensure that the steady-state coil bobbin temperature remains near room temperature for at least 4 hours of operation under constant 20W power input to the actuator. The performance of the TMS was evaluated experimentally and the results are presented in Fig. 10.

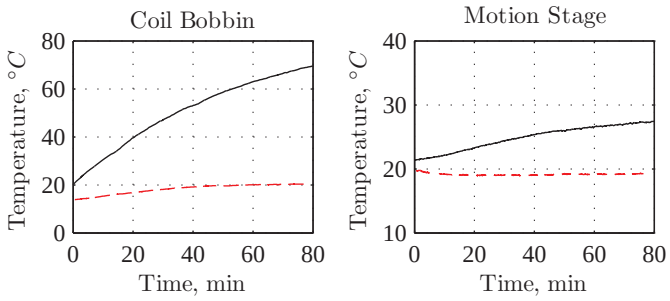

Figure 10. TEMPERATURE RISE OF THE COIL BOBBIN AND THE MOTION STAGE WITH (– –) AND WITHOUT (——) THE THERMAL MANAGEMENT SYSTEM.

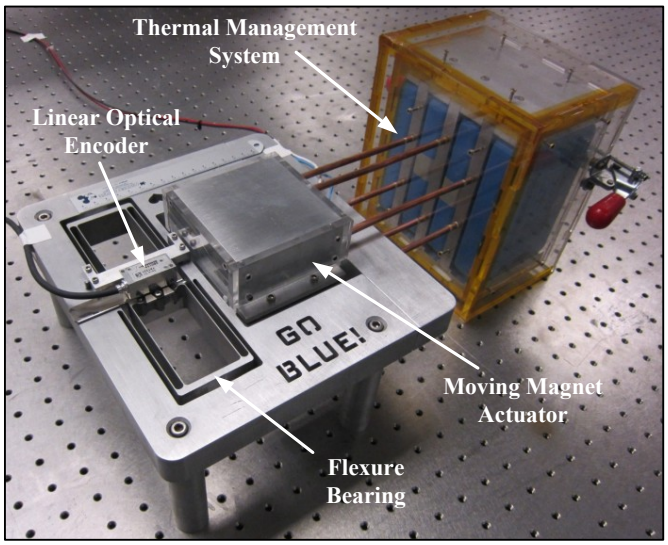

Figure 11. SINGLE-AXIS NANOPOSITIONING SYSTEM PROTOTYPE.

EXPERIMENTAL SETUP

In order to test the MMA, a single-axis symmetric double-parallelogram flexure bearing was designed and fabricated to provide frictionless and backlash-free motion guidance over the entire range of motion (Fig. 11). The minimum beam thickness and maximum beam depth were limited by the capability of the water-jet machining process and were set to be 0.75mm and 25.4mm, respectively. The beam length was chosen to be 80mm to provide $\pm$5mm motion range with a motion direction stiffness of 3.43N/mm. This resulted in a maximum force requirement of 17N.

The negative (destabilizing) stiffness of the off-axis force between the magnet and the back iron was determined via FEA to be 1.3N/mm near the nominal equilibrium position. The stiffness of the bearing perpendicular to the motion direction was determined to be 149.6N/mm (in-plane) and 70.6N/mm (out-of-plane), respectively, thereby ensuring the off-axis stability of the magnet-back iron assembly.

A current driver, based on a low noise power OpAmp MP111 from Cirrus Logic, was built to provide direct control of the actuation force, which enables a greater actuation bandwidth. The gain and the bandwidth of the amplifier were set to be 0.1A/V and 1KHz, respectively. An off-the-shelf high resolution linear optical encoder (RELM scale, Si-HN-4000 Readhead, and SIGNUM Interface from Renishaw) was used for position measurement and feedback. The key engineering specifications of the motion system are given in Table 2.

POSITIONING PERFORMANCE

Although the motion system presented above is physically capable of simultaneously producing large motion range and high motion quality, its ultimate positioning performance is dependent on the performance of a closed-loop control system.

Table 2. MOTION SYSTEM: KEY ENGINEERING SPECIFICATIONS.

Specifications	Value	Units
Motion Range	$\pm$5	mm
Force Constant	30-32	N/A
Resistance	43.6	Ω
Total Moving Mass	0.148	Kg
Stiffness	3.43	N/mm
Max. Continuous Power	15	W
Encoder Resolution	30	nm (pp)

In order to design a closed-loop controller, first, the open loop dynamic response of the nanopositioning system was found experimentally via broadband FFT-based system identification technique using a dynamic signal analyzer (SigLab, Model 20-22A). The set-up consisted of the current amplifier, MMA, flexure bearing and the position sensor. A band-limited chirp excitation was used within the frequency range of 1Hz to 1KHz. Figure 12 shows the resulting transfer function between the MMA coil current and the motion stage displacement. The open-loop bandwidth (-3dB) of the nanopositioning system is about 36Hz.

A lead-lag controller was designed to achieve good steady-state performance and stability margins. The control system was implemented on a real-time controller PXI-8106 from National Instruments equipped with PXI-6289 data acquisition card. The sampling rate was fixed at 5KHz. The prototype was tested for its point-to-point positioning performance with step commands of 2.5mm and 20nm, and the response in shown in Fig. 13. The steady-state positioning noise was found to be less than 4nm (RMS) over a 10mm motion range.

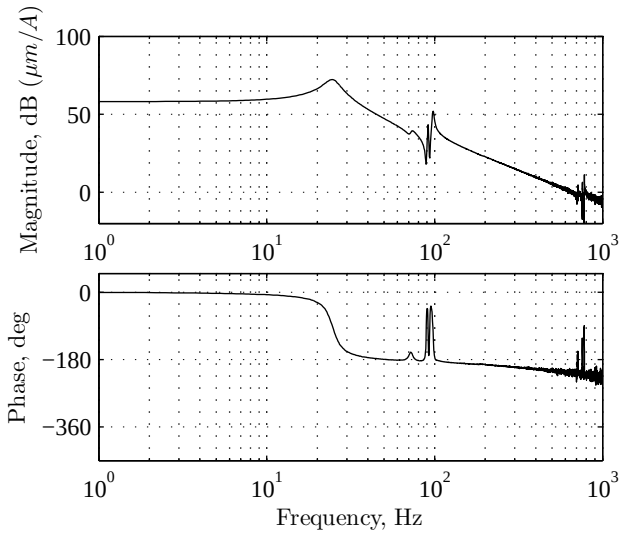

Figure 12. EXPERIMENTALLY OBTAINED OPEN LOOP FREQUENCY RESPONSE.

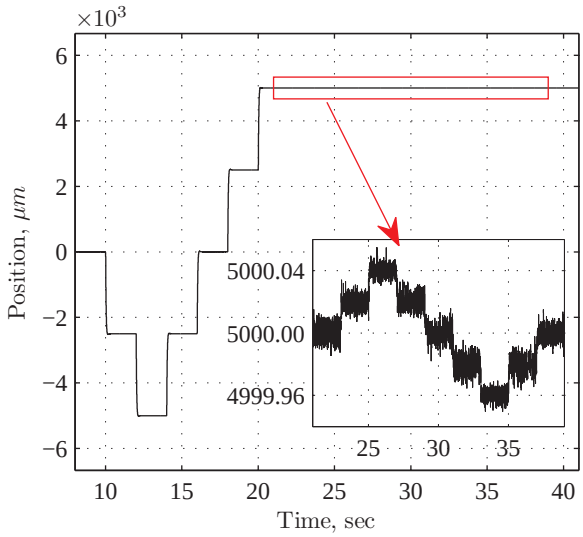

Figure 13. MOTION STAGE RESPONSE TO 2.5MM AND 20NM STEP COMMANDS.

CONCLUSION AND FUTURE WORK

This paper presents the design, fabrication, and testing of a moving magnet actuator along with a flexure bearing for large range nanopositioning systems. Some important system-level performance criteria and trade-offs are highlighted. It is shown that for a given MMA architecture, the actuation force remains directly proportional to the square root of the actuator moving mass and the square root of power consumed, irrespective of the scale of the actuator. A new performance metric for the MMA, β, which limits the open loop bandwidth of the overall motion system, is introduced. The geometry of the MMA – in particular, the dimensions of the magnet and the coil – was designed in a systematic manner to maximize the force output per unit square root of power consumed (4.56 N/$\sqrt{\text{W}}$), while minimizing the actuator moving mass (106g). The corresponding β value for the MMA is $14\sqrt{\text{Hz}}$. The thermal management system, incorporated as a part of the actuator, greatly abates the heat dissipation problem associated with MMAs. The MMA was tested for its point-to-point positioning performance with a double parallelogram flexure bearing and custom-made current driver. Preliminary results show promise for the MMA to be used as an actuator for large range nanopositioning systems. Future work will include: I. Derivation of an accurate closed-form model of the magnetic circuit of the MMA. II. Development of novel MMA architectures that provide greater values of β, thus paving the path for further performance improvements.

REFERENCES

[1] Yamada, T., et al., 1994. "A high-performance and low-profile moving-magnet actuator for disk drives". *IEEE Trans. on Magnetics,* **30**(6), pp. 4227–4229.

[2] Braune, S., and Liu, S., 2005. "Design of a novel moving magnet linear motor for use as a valve actuator". In 31st Annual Conference of the IEEE Industrial Electronics Society, IEEE, pp. 2041–2046.

[3] Banik, R., and Gweon, D. G., 2007. "Design and optimization of voice coil motor for application in active vibration isolation". *Sensors and Actuators, A: Physical,* **137**(2), pp. 236–243.

[4] Sinno, A., et al., 2007. "Enlarged atomic force microscopy scanning scope: novel sample-holder device with millimeter range". *Review of Scientific Instruments,* **78**(9), pp. 1–7.

[5] Gaoliang, D., et al., 2004. "Metrological large range scanning probe microscope". *Review of Scientific Instruments,* **75**(4), pp. 962–9.

[6] O'Brien, W., 2005. "Long-range motion with nanometer precision". *Photonics Spectra,* **39**(6), pp. 80–81.

[7] Awtar, S., and Parmar, G., 2010. "Physical and control systems design challenges in large range nanopositioning". In IFAC Sym. on Mechatronic Systems, Cambridge, MA.

[8] Hubbard, N. B., et al., 2006. "Actuators for micropositioners and nanopositioners". *Applied Mechanics Reviews,* **59**(6), pp. 324–334.

[9] Yao, B., et al., 2007. "Precision motion control of linear motor drive systems for micro/nano-positioning". Vol. B of *Int. Conference on Integration and Commercialization of Micro and Nanosystems*, ASME, pp. 1605–14.

[10] Tat Joo, T., et al., 2008. "A flexure-based electromagnetic linear actuator". *Nanotechnology,* **19**(31), pp. 315501–10.

[11] Youm, W., et al., 2008. "Control of voice coil motor nanoscanners for an atomic force microscopy system using a loop shaping technique". *Review of Scientific Instruments,* **79**(1), pp. 013707–6.

[12] Awtar, S., and Parmar, G., 2010. "Design of a large range XY nanopositioning system". In Proc. of IDETC/CIE, Montreal, Canada, Paper No. 28185.

[13] Fukada, S., and Nishimura, K., 2007. "Nanometric positioning over a one-millimeter stroke using a flexure guide and electromagnetic linear motor". *Int. Journal of Precision Engineering and Manufacturing,* **8**(2), pp. 49–53.

[14] Marcos, T., 2000. "The straight attraction: part one". *Motion Control Magazine*, June 2000.

[15] Vrijsen, N. H., et al., 2010. "Comparison of linear voice coil and reluctance actuators for high-precision applications". In 14th International Power Electronics and Motion Control Conference, IEEE Computer Society, pp. S329–36.

[16] Bolton, H. R., 1994. "Design aspects of electromagnetic actuators". In IEE Colloquium on Magnetic Materials for Sensors and Actuators, Vol. 6, pp. 1–5.

[17] Freudenberg, J. S., and Looze, D. P., 1988. *Frequency Domain Properties of Scalar and Multivariable Feedback Systems*. Springer-Verlag, Berlin.

[18] Stupak, J., Jr., and Gogue, G., 1989. "Voice-coil actuators: insight into the design". In 16th International Intelligent Motion Conference, Intertec Commun, pp. 241–53.